

# Texture evolution during equal channel angular extrusion Part I. Effect of route, number of passes and initial texture

S. Ferrasse<sup>a,\*</sup>, V.M. Segal<sup>a</sup>, S.R. Kalidindi<sup>b</sup>, F. Alford<sup>a</sup>

<sup>a</sup> Honeywell Electronic Materials, 15128 East Euclid Avenue, Spokane, WA 99216, USA

<sup>b</sup> Department of Materials Engineering, Drexel University, 32nd Chesnut Street, Philadelphia, PA 19104, USA

Received 4 July 2003; received in revised form 8 September 2003

---

## Abstract

It is shown that equal channel angular extrusion (ECAE) is an effective technique to control texture of metals and alloys. Two processing parameters, the route and number of passes, exert an important influence on texture evolution. Routes define orientations allowing the creation of numerous new components. Before four passes, depending on route and initial texture strength, all types of texture strength, from weak to very strong, are created, whereas after four passes, a global texture weakening is observed for all routes and medium to very weak textures are produced. A simple Taylor model shows that crystallographic slip mechanically activated by simple shear is the governing mechanism for evolution of texture orientations. However, after four passes, the creation of submicron-grained structures with high misorientations is believed to limit crystallographic slip and weaken textures.

© 2003 Published by Elsevier B.V.

*Keywords:* Equal channel angular extrusion; Texture of metals and alloys; Taylor model

---

## 1. Introduction

Submicron-grained (SMG) materials (with a grain size less than 1  $\mu\text{m}$ ) are attractive technical alternatives because they exhibit unusual physical and mechanical properties [1,2]. Intensive plastic deformation has been proven as an effective method to produce SMG materials. Several techniques are capable of achieving the required strain levels [3–5]. Of particular interest, the method of equal channel angular extrusion (ECAE) allows for the production of bulk pieces of SMG materials by simple shear [6–8]. Microstructures and properties of ECAE processed materials have been of high interest for the last 5 years [8–16]. Very fine grain sizes ( $<1 \mu\text{m}$ ) result in unusual effects such as ideal plastic behavior, high strength, enhanced ductility and toughness, and low temperature superplasticity. Recently some studies have focused on textures of ECAE deformed metals [17–37]. Texture analysis is of great relevance to mechanisms of grain refinement during ECAE. At this stage a few particular textures corresponding to various cases of ECAE deformation and die angles have been investigated

or modeled. The intent of this paper is to present a systematic study of texture formation in materials subjected to room temperature ECAE processing with a die angle of  $90^\circ$  and various numbers of passes and routes. This study clarifies the potential of ECAE technology to control texture.

## 2. Experimental

### 2.1. Original material and ECAE processing

High purity Al0.5Cu alloy was initially cast, homogenized and solutionized. This single phase, high stacking fault energy (SFE) alloy is a convenient material to analyze texture evolution under processing. All samples were submitted to two ECAE passes via route C [10–12] followed by annealing at  $250^\circ\text{C}$ , 1 h in order to produce an uniform and strong original texture with a recrystallized grain size of  $60 \mu\text{m}$ . Also, some samples were subsequently deformed by four passes route C and annealed at  $300^\circ\text{C}$ , 1 h to produce a weak texture with a recrystallized grain size of  $100 \mu\text{m}$ . Because of significant interest in texture development for flat products, ECAE was performed for flat billets (Fig. 1) [38,39]. A

---

\* Corresponding author.

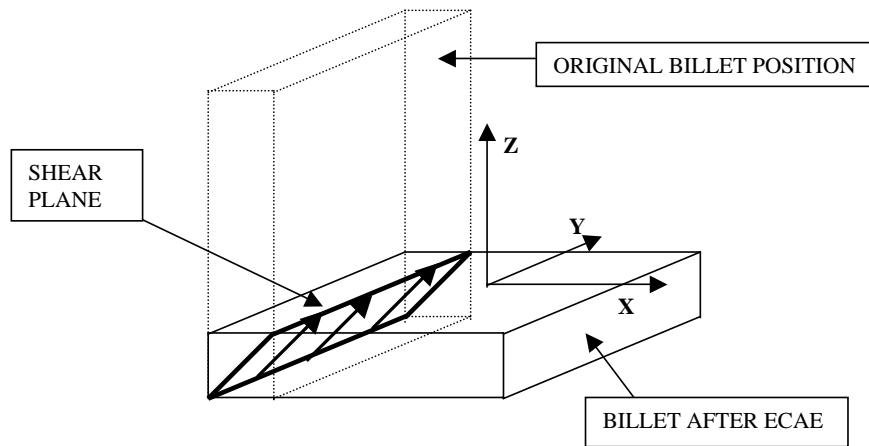


Fig. 1. ECAE of flat billet.

special note should be added on the definition of processing routes for this case. Different routes, which define selected shear planes and directions, may be attained by billet rotations about axis  $x$ ,  $y$  or  $z$  (Fig. 1) at subsequent passes. Similarly to the elongated billets that are usually studied [40], in route A, no change in billet orientation occurs between each pass. In route B, the sample is alternatively rotated  $\pm 90^\circ$  about  $z$  axis at each pass (Fig. 1). In route D, the sample is rotated continuously  $+90^\circ$  about the  $z$  axis at each pass. In route C, the sample is continuously rotated  $+180^\circ$  about the  $z$  axis.<sup>1</sup> Note that  $z$  axis is the rotation axis of route B and D for flat billet instead of the  $x$  axis for elongated billet. For the strong initial texture, routes A, B and D were studied for number of passes 1, 2, 3, 4, 6 and 8 and, for route C, all passes from one through eight were observed. For the weak initial texture, only experiments via routes A and D from one to four passes were done. ECAE experiments were performed at room temperature and a low ram speed ( $\approx 0.75$  mm/s). The processing of each route was carefully controlled. Well lubricated  $75 \text{ mm} \times 75 \text{ mm} \times 15 \text{ mm}$  samples were processed in a die with sharp corners and angle of  $90^\circ$  (Fig. 1) that corresponds to a true strain per pass  $\varepsilon = 1.16$ .

## 2.2. Texture measurement

Measurements of crystallographic texture were obtained with a Phillips X'Pert diffractometer. Textures were investigated along the mid-thickness of a billet section parallel to the  $x$ - $y$  plane (Fig. 1). Partial pole figures on the  $\{111\}$ ,  $\{200\}$  and  $\{220\}$  planes were generated. The Beartex software [41] was used to process the raw data, correct each pole figure for background and defocusing, and calculate the orientation distribution function (ODF) [41–43]. An analy-

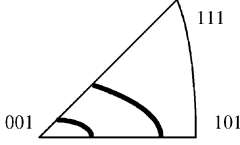
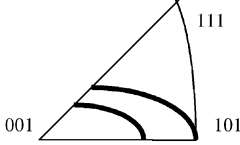
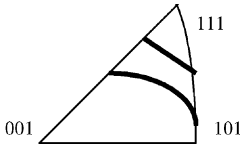

sis of fibers (orientation tubes) was performed by examining the ODF at constant values  $\gamma$  of 0, 5, 10, 15, 20, 22.5, 25, 30, 35, 40 and 45 according to the Roe/Matthies convention preferred in Beartex with Euler angles  $\alpha$ ,  $\beta$ ,  $\gamma$  (see Table 1). Also, Beartex (option COMP) estimates the integral intensity of the orientation distribution (OD) inside a given sphere in the orientation space that represents the volume fraction of grains possessing a given orientation inside the chosen sphere. A  $5^\circ$  spread around the component was considered. Texture or OD index, which is the root-mean-squared (RMS) value of peak ODF, was also used to evaluate texture strength [44,45]. It was assumed that OD index between 1 and 3 times random (t.r.) corresponds to random-to-weak textures, between 3 and 5 t.r. corresponds to weak-to-medium textures, between 5 and 20 t.r. corresponds to medium-to-strong textures and above 20 t.r. corresponds to extremely strong textures. Finally, for each pole figure, the extrusion axis of the last pass ( $x$  axis in Fig. 1) is always oriented along the  $x$  direction indicated in Fig. 4, and a perpendicular to the plane of pole figure is parallel to  $z$  axis in Fig. 1.

## 2.3. Texture modeling

A computer code based on a Taylor type crystal plasticity model was used to predict texture for simple shear deformation [45,46]. It is applicable at low homologous temperatures where plastic deformation is mainly accomplished by crystallographic slip. Other deformation mechanisms such as shear banding, twinning, grain boundary sliding and rotation, as well as effects of grain shape and size, are not taken into consideration. Despite this simplicity, it was found that the model provides reasonable predictions for texture evolution in single-phase, from medium to high stacking fault energy cubic metals whatever the deformation mode [45,46]. In simulations, 300 and 100 orientations were chosen to generate the weak (near random) and strong original textures, respectively.

<sup>1</sup> Some authors use the term  $B_A$  for route B and  $B_C$  for route D. In this case, routes B and D are not presented as basic routes but rather as dependent of routes A and C.

Table 1  
Basic description in the ODF space and inverse pole figure of principal fibers encountered for each route

Major types of Fxy fiber	Limits of location of fiber in (001) inverse pole figure (spreading due to ECAE route/pass).	Name of fiber for each route ( $x$ = name of route)	Range of Euler angles ( $\alpha$ $\beta$ $\gamma$ ) (for typical ODF $\gamma$ -cross sections) and corresponding range of plane
Fx1		FA1, FB1, FD1 FBD1 ( $N = 2$ for route B, D) FC1 (route C, $N$ odd)	$([215-255] [10-30] 0) = (106)-(102)$ , $([180-230] [10-25] 25) = (218)-(214)$ , $([135-190] [5-20] 45) = (118)-(113)$
		FC1 (route C, $N$ even)	$([220-255] [30-40] 0) = (203)-(101)$ , $([200-250] [20-40] 25) = (213)-(212)$ , $([180-190] [15-25] 45) = (115)-(112)$
Fx2		FA2, FB2, FC2, FD2	$([20-45] [40-50] 22.5) = (212)$ , $([350-15] [35-50] 45) = (223)-(334)$
Fx3		FA3, FB3, FC3, FD3, FBD3 ( $N = 2$ for routes B, D)	$([95-130] [15-35] 0) = (103)-(304)$ , $([90-120] [25-35] 15) = (7210)-(416)$ , $([80-110] [25-45] 25) = (213)-(212)$ , $([35-100] [20-35] 45) = (113)-(112)$

### 3. Results

#### 3.1. Initial textures

The strong initial texture (OD index = 21.7 t.r.) contains principally three major orientations (Table 2 for  $N = 0$ ). This atypical texture corresponds to the strongest textures encountered in traditional forming processes. The weak initial texture has an OD index of 2.6 t.r. (Table 2 for  $N = 0$ ).

#### 3.2. Evolution of texture orientation

Table 1 displays the definition of principal fibers found for each ECAE route. Tables 2–5 describe major orientations (with Euler angles  $\alpha$ ,  $\beta$ ,  $\gamma$  (Roe/Matthies) and corresponding  $\{xyz\}\langle uvw \rangle$  ideal description) and associated fibers. Texture orientation evolves similarly for both types of initial textures with some notable features.

First, starting texture exerts a limited influence by shifting or weakening orientations for one and two passes (Tables 2–5; see route A and D in Fig. 2a and b). At a higher number of passes, influence of the original texture on orientation disappears. For example, for three and four passes via route D (Fig. 2c and d) inverse pole figures exhibit similar orientations either for a strong or random initial texture.

Second, ECAE route has a tremendous impact on texture orientation especially at low number of passes. In fact, all orientations created with the four considered routes cover a significant area of the standard triangle (Tables 2–5,

Figs. 2–5). For example, with a strong initial texture, as many orientations as  $(102)\langle 241 \rangle$  (route A),  $(212)\langle 425 \rangle$  (route D),  $(416)\langle 413 \rangle$  (route C),  $(304)\langle 463 \rangle$  (route C) and,  $(7210)\langle 491 \rangle$  and  $(104)\langle 451 \rangle$  (route B) are created. Such orientations are fairly unusual compared to those obtained by traditional forming operations.

Third, ODF analysis indicates that a limited group of fibers containing one or several major orientations are associated with each route irrespective of number of passes and original texture (Tables 1–5; Fig. 6). The number of fibers varies from three to six but only one or two fibers are predominant for each route. These main fibers are noted FA3 and FA2 for route A (Fig. 6), FBD2 for routes B and D at two passes, FD1 for route D after three passes, FB3 and FB1 for route B after three passes, and FC3 and FC1 for route C (Table 1). The large number of fibers reflects the asymmetry of textures created during ECAE as evidenced by the  $(111)$  pole figure obtained after one pass for a random initial texture (Fig. 5b). Its patterns are similar to a plane rolling texture  $[19,45]$  with a rotation of  $10-15^\circ$  about  $y$  axis, which is directly responsible for the observed asymmetry. At a higher number of passes, textures remain planar and asymmetric and gradually different from the rolling case.

Fourth, there is also some similarity between the textures created by different routes as evidenced by pole figures (Figs. 5 and 6) and deformation fibers (Table 1). For a given fiber and  $\gamma$  cross-section in the ODF space, the effect of route on orientation is to change the angle  $\beta$  and, in a lesser extent, the angle  $\alpha$ . As a result, since angles  $\beta$  and  $\alpha$

Table 2  
Major orientations and corresponding fibers for route A

Number passes $N$	Major orientations ( <i>Notation</i> : Euler angles $(\alpha\beta\gamma):\{xyz\}\langle uvw \rangle$ ; % total volume with $5^\circ$ spread)	Corresponding fiber
Route A (strong initial texture)		
Original ( $N = 0$ )	(10.9 54.7 45): $(-1\ 1\ 1)\langle 1\ -2\ 3 \rangle$ : 16 (105 26.5 0): $(-1\ 0\ 2)\langle -2\ 8\ -1 \rangle$ : 14 (110 24 26.5): $(-2\ 1\ 5)\langle -5\ -5\ -1 \rangle$ : 9.3	
$N = 1$	(119 26.5 0): $(-1\ 0\ 2)\langle -2\ -4\ -1 \rangle$ : 17.62 (346 43.3 45): $(-2\ 2\ 3)\langle 2\ -1\ 2 \rangle$ : 7.62	FA3 FA2
$N = 2$	(138 26.5 0): $(-1\ 0\ 2)\langle -2\ -2\ -1 \rangle$ : 8.66 (31 36.7 26.5): $(-2\ 1\ 3)\langle 3\ -6\ 4 \rangle$ : 8.6	FA3 FA2
$N = 3$	(126.7 26.5 0): $(-1\ 0\ 2)\langle -2\ -3\ -1 \rangle$ : 7.45 (21 36.7 26.5): $(-2\ 1\ 3)\langle 2\ -4\ 3 \rangle$ : 6.1	FA3 FA2
$N = 4$	(26.5 36.7 26.5): $(-2\ 1\ 3)\langle 2\ -6\ 4 \rangle$ : 9.42 (138 26.5 0): $(-1\ 0\ 2)\langle -2\ -2\ -1 \rangle$ : 4.62 (169 15.8 45): $(-1\ 1\ 5)\langle -3\ 2\ -1 \rangle$ : 4.32	FA2 FA3 FA1
$N = 6$	(126.7 26.5 0): $(-1\ 0\ 2)\langle -2\ -3\ -1 \rangle$ : 6.66 (228 33.7 0): $(-2\ 0\ 3)\langle -3\ 4\ -2 \rangle$ : 5.8 (31 36.7 26.5): $(-2\ 1\ 3)\langle 3\ -6\ 4 \rangle$ : 3.42	FA3 FA1 FA2
$N = 8$	All major orientations $< 3.1$	
Route A (weak initial texture)		
$N = 0$	(80 25.2 45): $(-1\ 1\ 3)\langle -8\ -11\ 1 \rangle$ : 4.3	
$N = 1$	(0 46.7 45): $(-3\ 3\ 4)\langle 2\ -2\ 3 \rangle$ : 5.8 (222 26.5 0): $(-1\ 0\ 2)\langle -2\ 2\ -1 \rangle$ : 5 (128 18.4 0): $(-1\ 0\ 3)\langle -3\ -4\ -1 \rangle$ : 4.01	FA2 FA1 FA3
$N = 2$	(126.7 26.5 0): $(-1\ 0\ 2)\langle -2\ -3\ -1 \rangle$ : 6.22 (26.5 48.2 26.5): $(-2\ 1\ 2)\langle 1\ -2\ 2 \rangle$ : 5.4 (162 13.2 45): $(-1\ 1\ 6)\langle -4\ 2\ -1 \rangle$ : 5.4	FA3 FA2 FA1
$N = 4$	(233 26.5 0): $(-1\ 0\ 2)\langle -2\ 3\ -1 \rangle$ : 4.63 (136 19.5 45): $(-1\ 1\ 4)\langle -4\ 0\ -1 \rangle$ : 4.54 (26.5 36.7 26.5): $(-2\ 1\ 3)\langle 3\ -6\ 4 \rangle$ : 3.7	FA1 FA1 FA2

affect  $(xyz)$  plane and  $\langle uvw \rangle$  directions, respectively, either the major orientation inside a fiber changes or a new fiber with new orientation is produced. The specific denomination mentioned earlier takes into account these similarities. A fiber name has the form  $F_{xy}$ , where a letter  $x$  corresponds to the considered route (respectively A, B, C, D) and a number  $y$  corresponds to a specific set of angles  $\alpha, \gamma$ . Three major types of fibers  $F_{x1}$ ,  $F_{x2}$  and  $F_{x3}$  were identified as shown in Table 1. Each of these fibers exhibits similar values for the

set of angles  $\alpha, \gamma$  for most of the routes and passes (for example, from around (230, 0) to (180, 45) for  $F_{x1}$  (Table 1)), but specific values of angles  $\beta$  and, to some extent,  $\alpha$  depend on deformation path. Table 1 shows the area of the inverse pole figure as well as the range of planes and Euler angles covered by each of these major fibers (for example,  $F_{x1}$ , when regrouping all studied routes corresponding to FA1, FB1, FC1, FD1 and FBD1 fibers). Fig. 6 shows fibers FA1, FA2 and FA3 in ODF space after the first pass.

Table 3  
Major orientations and corresponding fibers for route B

Number of passes $N$	Major orientations ( <i>Notation</i> : Euler angles $(\alpha\beta\gamma):\{xyz\}\langle uvw \rangle$ ; % total volume with $5^\circ$ spread)	Corresponding fiber
Route B (strong initial texture)		
$N = 2$	(0 48 2 6.5): $(-2\ 1\ 2)\langle 4\ 2\ 5 \rangle$ : 24.24 (216 15.8 45): $(-1\ 1\ 5)\langle -2\ 4\ -1 \rangle$ : 8.07 (138 26.5 0): $(-1\ 0\ 2)\langle -2\ -2\ -1 \rangle$ : 5.04	FBD2 FBD1 FBD3
$N = 3$	(260 36 74): $(-2\ 7\ 10)\langle 9\ 4\ -1 \rangle$ : 15.49 (118 18.4 90): $(0\ 1\ 3)\langle -6\ 3\ -1 \rangle$ : 5.23	FB3 FB1
$N = 4$	(100 36 16): $(-7\ 2\ 10)\langle -4\ -9\ -1 \rangle$ : 12 (230.5 14 0): $(-1\ 0\ 4)\langle -4\ 5\ -1 \rangle$ : 8.05	FB3 FB1
$N = 6$	(230.5 14 0): $(-1\ 0\ 4)\langle -4\ 5\ -1 \rangle$ : 12.46 (100 36 16): $(-7\ 2\ 10)\langle -4\ -9\ -1 \rangle$ : 10.2	FB1 FB3
$N = 8$	(230.5 14 0): $(-1\ 0\ 4)\langle -4\ 5\ -1 \rangle$ : 9.19 (180 13.2 45): $(-1\ 1\ 6)\langle -3\ 3\ -1 \rangle$ : 8.21 (100 36 16): $(-7\ 2\ 10)\langle -4\ -9\ -1 \rangle$ : 7.48	FB1 FB1 FB3

Table 4  
Major orientations and corresponding fibers for route C

Number of passes $N$	Major orientations (Notation: Euler angles $(\alpha\beta\gamma):\{xyz\}\{uvw\}$ : % total volume with $5^\circ$ spread)	Corresponding fiber
Route C (strong initial texture)		
$N = 2$	(0 34.5 14): (-4 1 6)(4 -1 3): 43.3 (221.8 265 0): (-1 0 2)(-2 2 -1): 10.5	FC3 FC1
$N = 3$	(254 18.4 0): (-1 0 3)(-3 11 -1): 7.5 (111.5 46.5 18.4): (-3 1 3)(-2 -3 -1): 6.6	FC1 FC3
$N = 4$	(130 36.9 10): (-3 0 4)(-4 -6 -3): 15.05 FC1 < 3.75	FC3 FC1
$N = 5$	(270 14 0): (-1 0 4)(0 1 0): 4.66 (26.5 48 26.5): (-2 1 2)(1 -2 2): 2.54	FC1 FC3
$N = 6$	(110 36 16): (-7 2 10)(-5 -8 -2): 11.6 (234 33.7 0): (-2 0 3)(-3 5 -2): 5.7	FC3 FC1
$N = 7$	(242 18.4 0): (-1 0 3)(-3 6 -1): 4.66 (188 11.4 45): (-1 1 7)(-3 4 -1): 3.36	FC1 FC3
$N = 8$	(136.5 18.4 0): (-1 0 3)(-3 3 1): 14.71 (257 45 0): (-1 0 1)(-8 49 -8): 8.75	FC3 FC1

Fifth, for any route, less variation in orientation is seen as the number of passes  $N$  augments. Some principal fibers and orientations are gradually selected and conserved as  $N$  increases. Texture evolution can then be described by simple rules, which show how processing macromechanics influences texture:

- For *route A*, material distortion is close to monotonic, which results in a few gradual changes in orientations (Figs. 2 and 5, Table 2). Mainly, the same planes, (1 0 2) and (2 1 3), are involved. This type of linear evolution is similar to that found in rolling;
- For *route D*, after three passes, no significant changes in the ODF or pole figure is observed whatever the original texture (Fig. 2; Table 5). This status quo can be surprising since a rotation of  $90^\circ$  is continuously done at each pass.

However, for each pole figure or ODF, the extrusion direction at the last pass  $N$  serves as reference and therefore is rotated  $90^\circ$  compared to pass  $N - 1$ ;

- For *route B*, a special evolution is noticed. After three passes, there is no significant changes in major components although pole figure patterns appear different (Fig. 4; Table 3). In fact, the pole figures corresponding to odd numbered of passes can be approximately deduced from those corresponding to even numbered of passes by a mirror symmetry, whose plane is indicated in Fig. 4. This cyclic evolution is related to the constant  $\pm 90^\circ$  rotation imposed to billet in route B;
- *Route C* is the most atypical (Fig. 3; Table 4). Textures should tend to come back to the original strong texture for even numbered passes because simple shear is inverted at each subsequent pass. However, due to the constraints

Table 5  
Major orientations and corresponding fibers for route D

Number of passes $N$	Major orientations (Notation: Euler angles $(\alpha\beta\gamma):\{xyz\}\{uvw\}$ : % total volume with $5^\circ$ spread)	Corresponding fiber
Route D (strong initial texture)		
$N = 2$	(0 48 26.5): (-2 1 2)(4 2 5): 24.24 (216 15.8 45): (-1 1 5)(-2 4 -1): 8.07 (138 26.5 0): (-1 0 2)(-2 -2 -1): 5.04	FBD2 FBD1 FBD3
$N = 3$	(197 20.4 26.5): (-2 1 6)(-2 2 -1): 9.57 Major orientation in FD2, FD6, FD3 < 3	FD1
$N = 4$	(222 26.5 0): (-1 0 2)(-2 2 -1): 13.34 FD2, FD3, FD6 < 3.8	FD1
$N = 6$	(223.5 18.5 0): (-1 0 3)(-3 3 -1): 7.4 Major orientation in FD3, FD2, FD6 < 2.5	FD1
$N = 8$	Major orientation in FD1, FD2, FD3 < 3.5	
Route D (weak initial texture)		
$N = 2$	(241 26.5 0): (-1 0 2)(-2 4 -1): 12.72 (26.5 48.2 26.5): (-2 1 2)(1 -2 2): 4.1	FBD1 FBD2
$N = 3$	(197 20.4 26.5): (-2 1 6)(-2 2 -1): 8.8 (26.5 48.2 26.5): (-2 1 2)(1 -2 2): 3.9	FD1 FD2
$N = 4$	(221.8 26.5 0): (-1 0 2)(-2 2 -1): 7.2 (26.5 48.2 26.5): (-2 1 2)(1 -2 2): 3.1	FD1 FD2

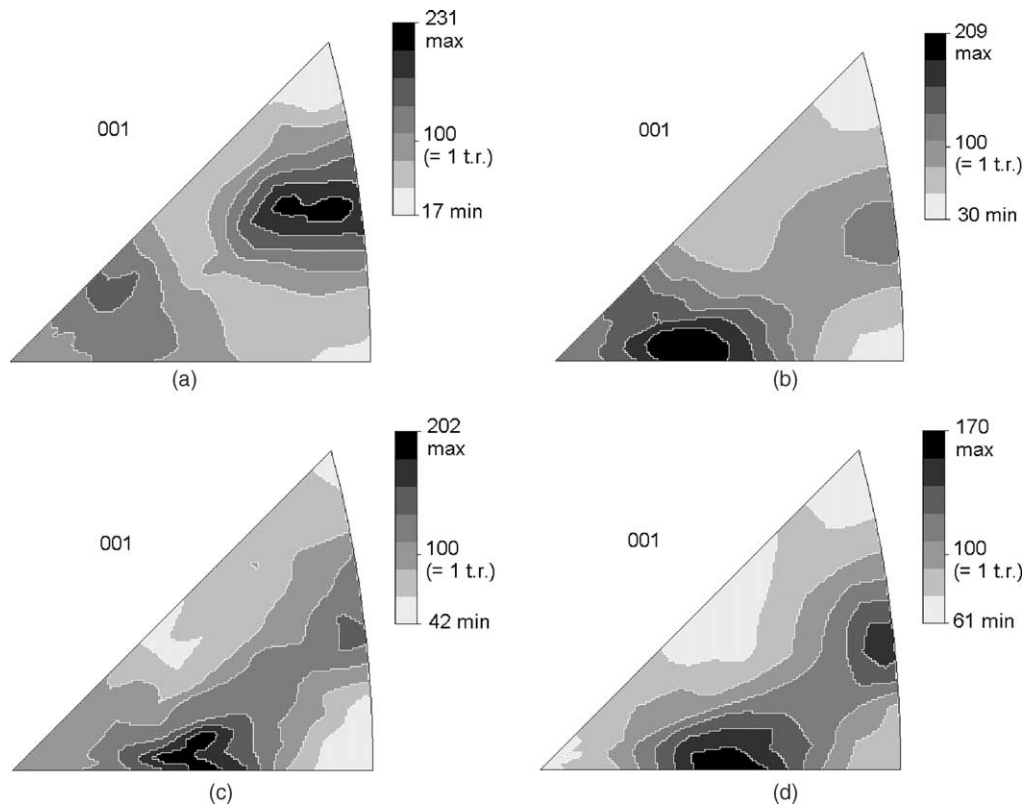


Fig. 2. Inverse (001) pole figures for route D after two passes for a strong (a) and weak (b) initial texture, and after four passes for a strong (c) and weak (d) initial texture.

imposed by grain structure and deformation history, the restoration at pass  $N$  of texture at pass  $N - 2$  is never fully realized. Instead, slightly new types of textures are permanently created due to the influence of a strong hysteresis phenomenon. As shown in Fig. 3, for  $N = 3, 5$  and  $7$ , main planes are close to the (1 0 3) and (2 1 2), whereas for  $N = 2, 4, 6$  and  $8$ , main planes are located around (7 2 10)–(3 0 2). Similarly, strength of major fibers, FC1 and particularly FC3, alternates (Table 4). However hysteresis decreases in amplitude after  $N = 5$  (Table 4).

### 3.3. Evolution of texture strength

Study of texture strength reveals several points evidenced in Fig. 7a.

First, starting texture impacts greatly texture strength at a low number of ECAE passes. For any route, the stronger the original texture, the stronger the texture for a few ECAE passes as shown by OD index and percentage volume of major components (Fig. 7a; Tables 2–5). At high strains, after three or four passes, the influence of original texture on texture strength diminishes markedly.

Second, there is a general decrease in texture strength as the number of passes increases. OD index, maximum in pole figures or volume percentage of orientations diminish clearly (Tables 2–5; Fig. 7a). For a weak initial texture, the strongest textures (of a medium type) are created at one and two passes

for route A or D; after three passes only, weak textures are present. For a strong initial texture, two areas can be distinguished. The sharpest changes and strongest textures are obtained before four passes, whereas, after four passes, variations in texture strength decrease and medium-strong to very weak textures are created depending on the route.

Third, the evolution of texture strength depends on the route. Routes A, B and D exhibit a rather continuous diminution of texture strength (Tables 2–5; Fig. 7a). Route D and A are the most effective for texture randomization after four passes with respective FD1 and FA1 fibers containing less than 4% of total volume. In route B, for a strong starting texture, it is still possible to obtain medium-strong textures after six and eight passes with OD index from 5 to 7 t.r. (Fig. 7a; Table 3). Route C again is special (Fig. 7a; Table 4) and exhibits a cyclic evolution in texture strength. Even after four passes, textures are very weak for odd numbered passes and rather strong for even numbered passes as shown by main orientations of fiber FC3, whose integral intensity oscillates between 12 and 14% and less than 5% (Table 4).

### 3.4. Modeling of texture orientation

In general, modeling provides good predictions of texture orientations for both strong and weak initial textures (Figs. 5 and 8). This confirms that ECAE deformation mode is simple shear. A closer match is found with a random starting

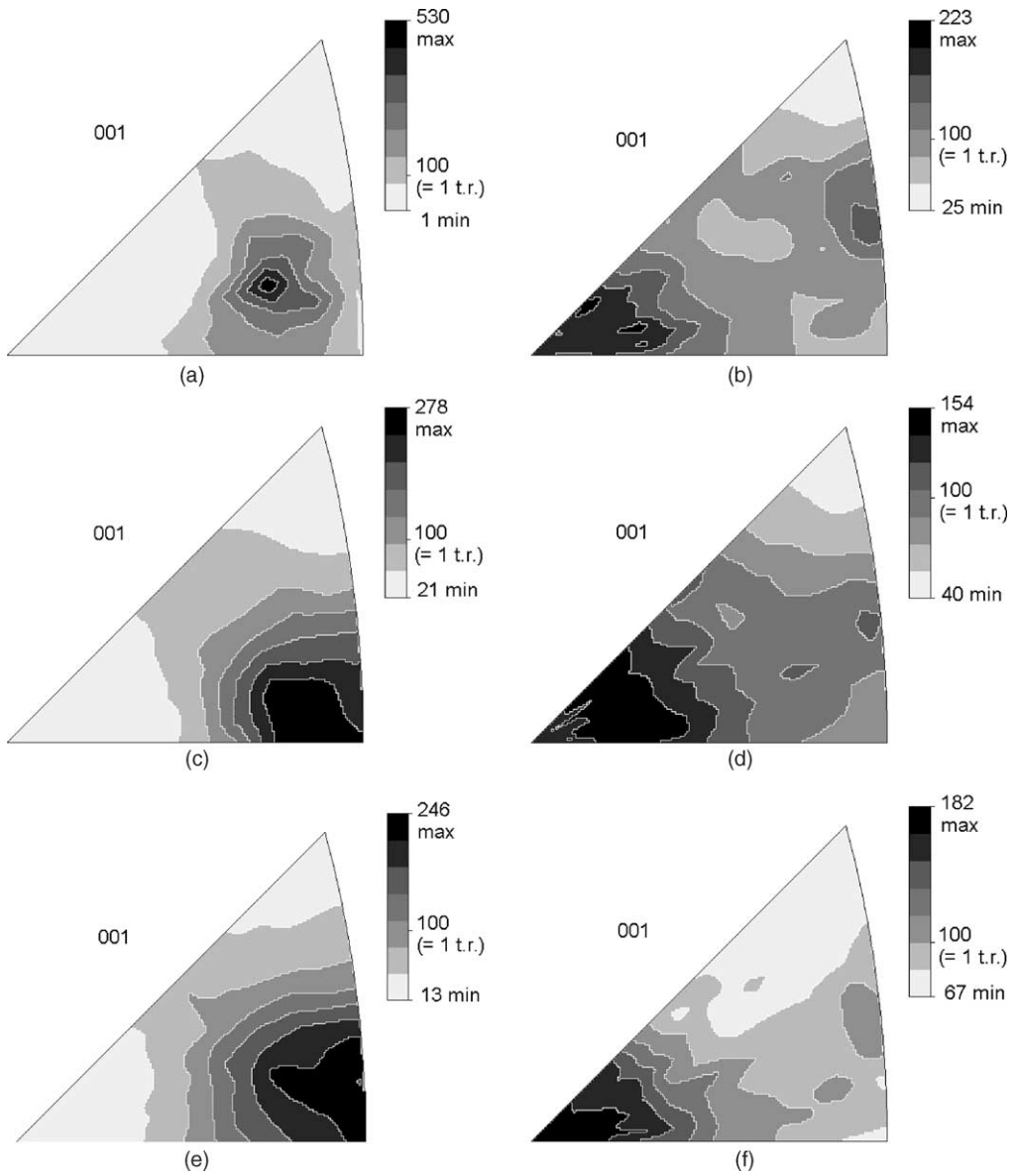


Fig. 3. Inverse (001) pole figures for route C after two (a), three (b), four (c), five (d), six (e) and seven (f) passes.

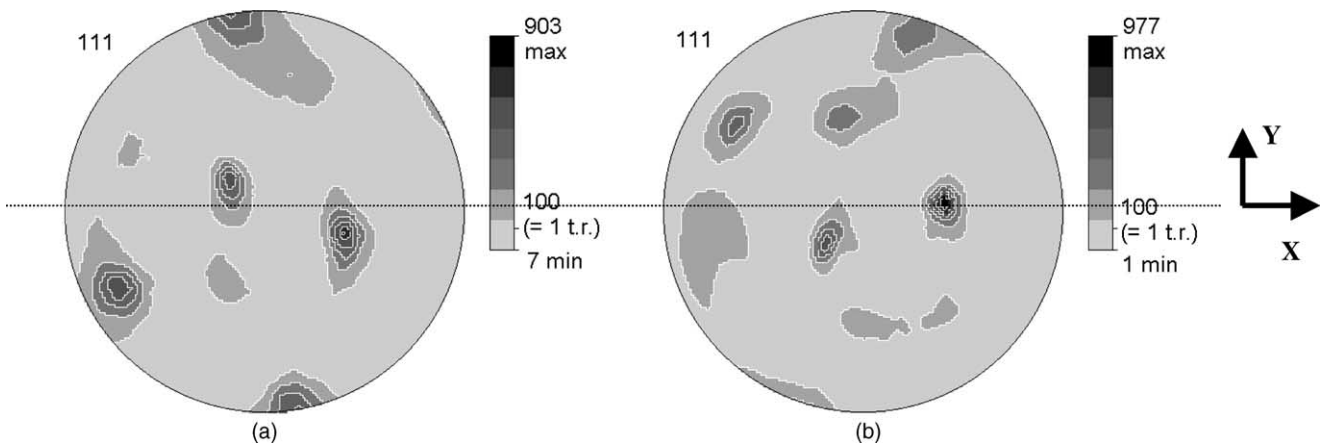


Fig. 4. (111) pole figures after three (a) and four (b) passes via route B for a strong initial texture.

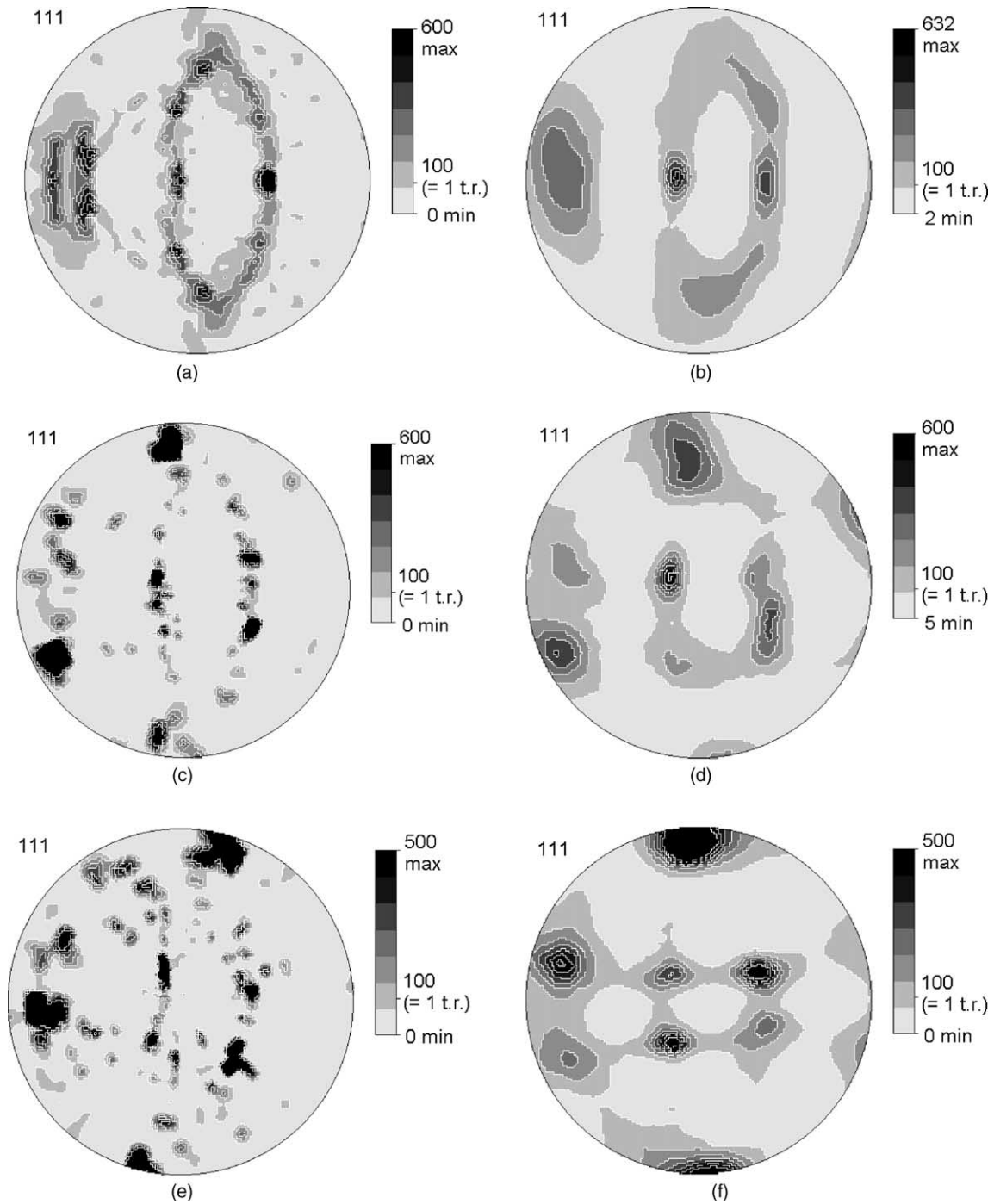


Fig. 5. Predicted by modeling (a, c, e) and experimental (b, d, f) (111) pole figures for (a), (b)—one pass for a weak initial texture; (c) (d)—four passes via route A for a strong initial texture; (e) (f)—four passes via route C for a strong initial texture.

texture because this texture was the easiest to generate and a larger number of orientations were considered during calculations. For example, for a random initial texture, a good correlation between experiments and simulation is obtained for route D up to three passes (compare Figs. 2b and 8a) and for route A up to four passes. Also major deformation fibers given by the model are FA2 and FA3 for route A, FC1 and FC3 for route C, FD1 and FD2 for route D, and FB1 and FB3 for route B. The Fx1 type of fiber runs from the (103)

plane to the (117) plane, Fx2 runs from the (212) to the (334)/(223) planes, and Fx3 contains (103) and (7210) as principal planes. Similar trends were experimentally observed for corresponding routes. Finally, modeling confirms the cyclic evolution of texture for route C.

Despite these successes, there are also discrepancies between modeling and experiments as the number of passes increases. For example, for route D at four passes, computer code selects planes (103) and especially (334) instead of



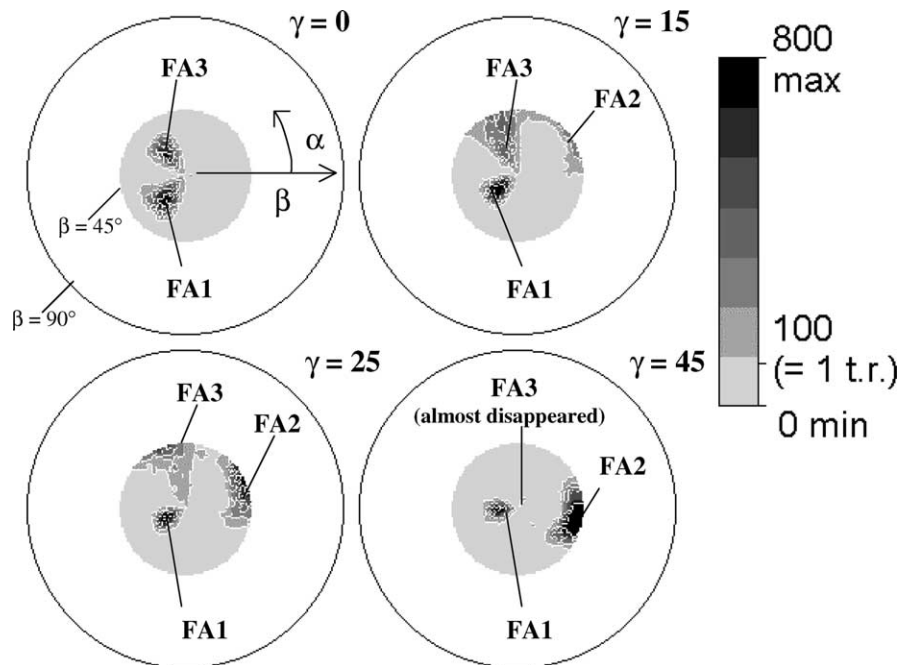


Fig. 6. Typical fibers after one pass for a weak initial texture. Partial ODF with the FA1, FA3 and FA4 fibers are represented according to the Roe/Matthies convention at four  $\gamma$ -sections ( $\gamma = 0, 15, 25, 45$ ), and for  $\alpha \in [0, 360]$  and  $\beta \in [0, 45]$ . The remaining part of ODF (i.e.  $\beta \in [45, 90]$ ) is not represented because of symmetry.

(1 0 3) and (2 1 2) obtained experimentally (compare Figs. 2d and 8b). More obvious variations are observable for a strong original texture (Fig. 5c–f). For route C, simulation is unable to reproduce the gradual textural changes imposed by hysteresis. In fact, there is rather an oscillation between two limit textures, the initial one and the one after one pass.

### 3.5. Modeling of texture strength

Simulation results on texture strength are shown on Fig. 7b. In all cases, simulation predicts much stronger textures than experiments. There is always a huge difference in the value of the OD index often by two and three orders in magnitude (compare Fig. 7a and b). Moreover, whatever the initial texture, a continuous strengthening is obtained for routes A, B and D when number of passes increases (Fig. 7b). This result is contradictory to the significant texture weakening observed experimentally (Fig. 7a).

## 4. Discussion

Experiments and modeling demonstrate that, to a great extent, ECAE provides the freedom to control texture orientation and strength. Two specific ECAE parameters, route and number of passes, are proven to be very efficient for such control. The influence of strong and near random initial textures was also studied. It is convenient to comment on these effects, first, on texture orientation and, second, on texture strength.

### 4.1. Evolution of texture orientation

Texture orientations are very sensitive to processing macro-mechanics as evidenced by simulation. The simple model based on Taylor theory shows that crystallographic slip, which is mechanically activated by simple shear along crossing plane of channels, is the major mechanism controlling texture development during ECAE as also shown in [21,25,26,28,33]. This explains the origin of fiber formation and the similarity between some fibers whatever the ECAE pass number or route. Due to the constraints imposed by simple shear, crystallographic slip selects a few energetically favorable stable orientations that all deformed grains tend to acquire, depending on their initial orientations. However, in polycrystalline aggregates, most of the grains find only the closest orientations to these “ideal” orientations. As a consequence continuous arrays of grains with close orientations, more precisely called fibers or tubes, are created inside the material. For a given material, such fibers depend on the deformation mode. Since ECAE develops simple shear at each pass whatever the route, similar sets of fibers are created. Simple shear is also responsible for the asymmetry of textures as evidenced by multiple sets of fibers [17–36].

Complexity in the evolution of orientations arises mainly as a function of ECAE route. Route is the most influential factor because it selects a group of shear planes and directions at each pass and activates them in a precise order [10–12]. Therefore, even if simple shear acts at each pass and tends to produce a same texture, the starting texture of

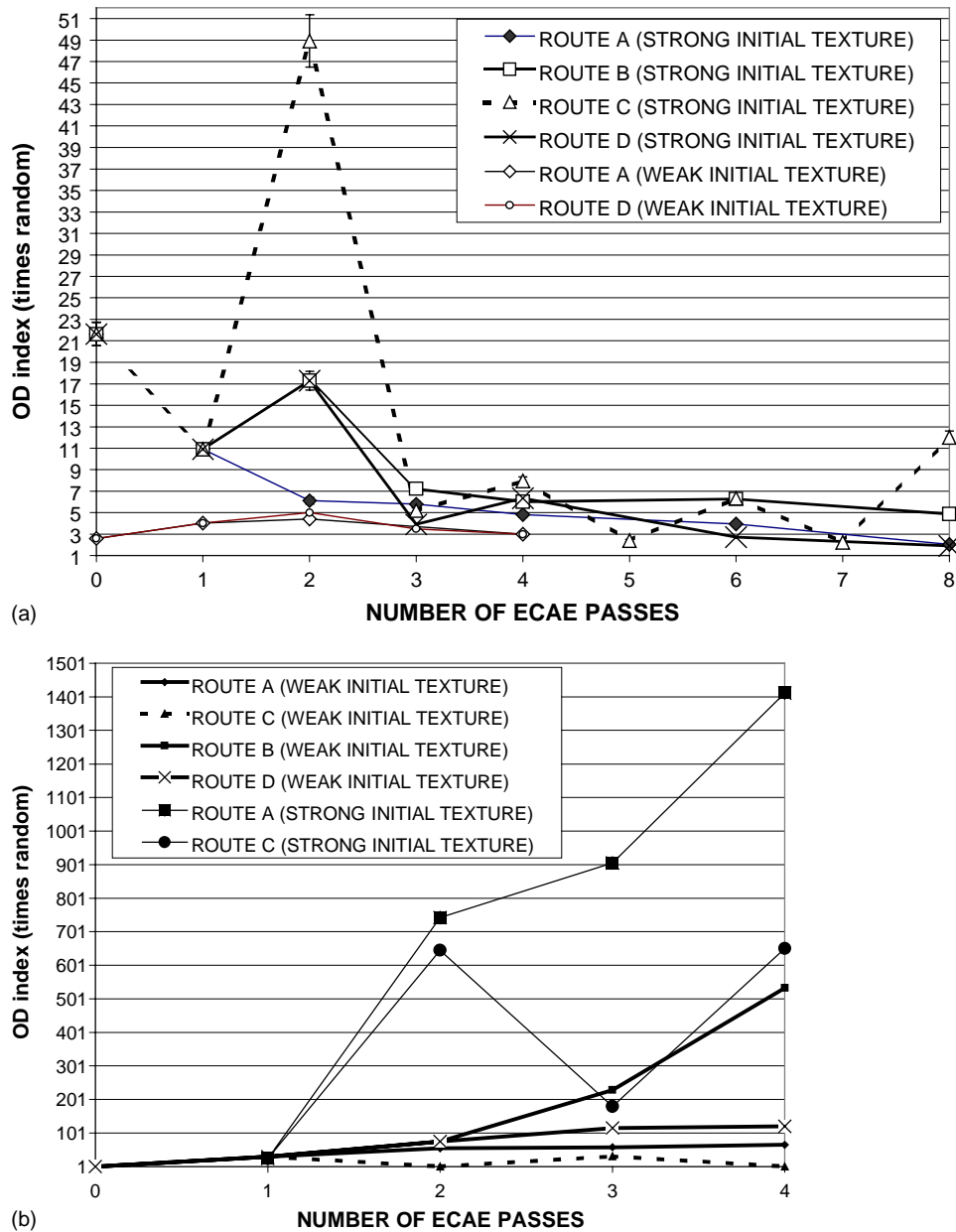


Fig. 7. Experimental (a) and modeling (b) OD indexes for a strong and weak initial textures as a function of number of passes via routes A, B, C and D.

a sample entering ECAE die at a pass  $N$  will differ between routes due the specific inter-pass rotations of each route. As a result, the end texture after completion of the  $N$ th pass differs for each route [22,25,27–29,33]. For route A, accumulated strain is close to monotonic and planar so that only a few gradual changes in texture orientations occur. Route C is a case of cyclic plane deformation, where shear direction is reversed at each pass along the same shear plane thereby giving rise to a cyclic textural evolution. Routes B and D involve non-monotonic cross-loading deformation in three dimensions [10,56]. The non-monotonic routes B, D and C give the most atypical and variable textural evolutions. The noticeable effects are (i) the main orientations within a fiber change at each pass; (ii) some fibers become predominant

at the expense of others; (iii) a fiber is partially or entirely modified. Since there is a multitude of combinations of processing routes, the opportunities to control texture are numerous. It is unlikely however to produce every possible orientation because crystallographic slip induced by simple shear will tend to select some particular orientations.

Compared to ECAE route, starting texture and number of passes have a limited effect on texture orientation. Initial texture plays a limited role for the first few passes ( $N = 1, 2, 3$ ) and its effect disappears for  $N > 3$ . A similar observation was made in [21]. It can be argued that the amount of deformation involved at each pass is so high ( $\epsilon = 1.16$ ) that any original influence is diminished. Even in route C, despite the inversion of simple shear and because of hysteresis, the

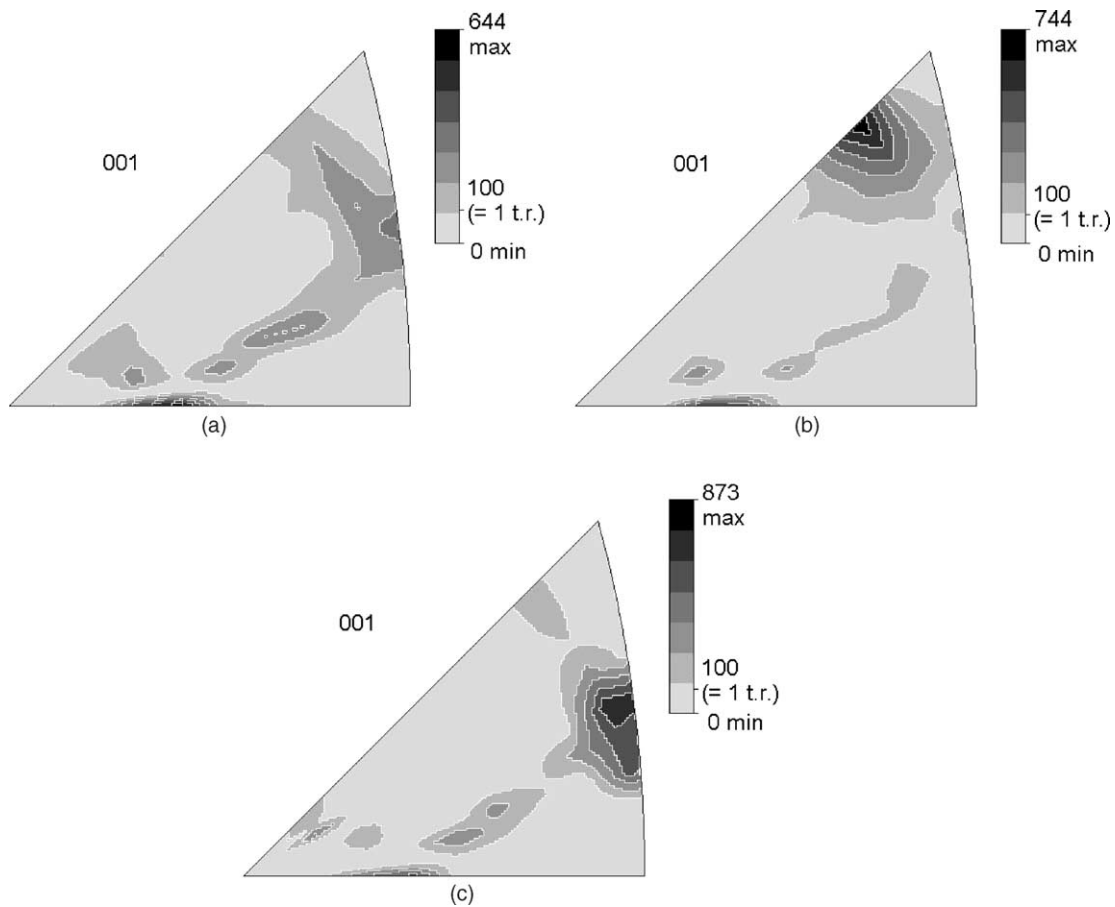


Fig. 8. Inverse (001) pole figures predicted by modeling for a weak initial texture after two passes via route D (a), four passes via route D (b), and four passes via route A (c).

components obtained after two passes differ from the original texture [22]. Finally, as the number of passes increases, especially after four passes, less change in texture orientation occurs. There is rather a global spreading around some final orientations for each route that results from texture weakening and structural transformations as explained below.

#### 4.2. Evolution of texture strength

A global weakening of texture from medium to very weak is observed as the number of passes augments, especially after three or four passes, whatever the initial texture. Textural randomization is enhanced by weaker initial textures [22], and, in decreasing order of influence, for routes D, A and C (in the last case for odd numbered passes). It is still possible to obtain medium-strong textures after four passes as shown in routes B or C (for even numbered passes) with a strong initial texture. Texture softening at increased passes was also found in [18,28,31,35]. Contrary to experiments, computer simulation predicts continuous texture strengthening for all routes when number of passes augments. Predictions in orientation also become less accurate at high strains. These contradictory results prove that crystallographic slip is not the only mechanism responsible for texture evolution

during ECAE [47,48]. In particular, the simple Taylor code does not consider all microstructural changes occurring during ECAE [28,45–48]. The abundant literature concerning ECAE [8–37,47,48] shows that at high strains, a sub-micron structure is created (see part II, Fig. 1). Break up and refinement of microstructures is induced mechanically by dynamic recrystallization, which is believed to involve mechanisms such as grain/subgrain rotation, flow localization in shear bands and their intersections [9,10,12,15,33,47–51]. These mechanisms contribute to diminish texture strength after three passes. Basically, the areas belonging to each fiber at first passes are divided into highly stressed and misoriented SMG structures, which disperse more X-rays and weaken fibers.

The occurrence of texture spreading at high deformations was reported for different processes including, for example, rolling after 90–95% reduction [44,52–55]. Most of these observations were made for strains, which were not as large as in this study. As ECAE extends plastic straining to very high levels, it is possible to create weak, almost random textures by promoting mechanically induced dynamic recrystallization.

In resume, ECAE was proven as an effective technique for grain refinement to sub-micron size in massive billets

by severe plastic deformation [8–37,47,48,52]. In terms of texture control, it appears the most promising to vary different routes for a low number of passes ( $N \leq 4$ ) and strong initial texture. The tool angle is also a possible parameter, which can affect texture [23–25]. Severe deformation ( $N \geq 4$ ) combined with optimal route is another attractive option to produce SMG materials with either very weak or medium-strong textures. However, a careful choice of ECAE processing characteristics must be attained in order to induce simple shear and control texture [56].

## 5. Conclusions

1. ECAE is an effective technique to control texture strength and orientation. Compared to conventional techniques ECAE offers a large variety of parameters for texture evolution. Two of them, the number of passes and the deformation route, are the most important.
2. Numerous orientations, which covers most of the areas of the standard triangle have been obtained. The ECAE route provides a radical and influential mechanism for texture transformation at a low number of passes ( $N \leq 4$ ).
3. All types of texture strength have been obtained by controlling the number of passes: from medium to very strong for a low number of passes ( $N < 4$ ) and from very weak, near random, to medium-strong for a large number of passes ( $N > 4$ ).
4. A simple Taylor model shows that crystallographic slip enhanced by simple shear is the major mechanism that defines texture orientation during ECAE. It explains reasonably well major orientations and fibers obtained for each route. A few classes of fibers, which are characteristic of the ECAE simple shear deformation mode were identified.
5. The Taylor model fails to predict texture strength because various mechanisms other than crystallographic slip become important at high levels of deformation. These mechanisms favor mechanically induced dynamic recrystallization and produce sub-micron grained structures, which tend to be weak and, in some cases, near random textures. Routes A and D are the most effective for texture randomization.
6. Initial texture plays a limited role on texture orientation and a significant role on texture strength at the earliest stage of deformation. For route C, its influence is the strongest.

## Acknowledgements

The authors wish to express appreciation to other contributors to this work, especially Prof. H.R. Wenk and Dr. D. Damodaran.

## References

- [1] R.W. Siegel, in: M. Nastasi, D.M. Parkin, H. Gleiter (Eds.), Proceedings of the NATO ASI Mechanical Properties of Ultrafine-Grained Materials, Quebec, 1993, p. 509.
- [2] C. Suryanarayana, Bull. Mater. Sci. 17 (1994) 307–346.
- [3] V.Y. Gertsman, R. Birringer, R.Z. Valiev, H. Gleiter, Scripta Metall. 30 (1994) 229–234.
- [4] H.J. Zughhaer, J. Nutting, Mater. Sci. Technol. 8 (1992) 1104–1107.
- [5] I. Saunders, J. Nutting, Met. Sci. 19 (1984) 571–575.
- [6] V.M. Segal, Invention Certificate of the USSR, No. 575,892 (1977).
- [7] V.M. Segal, V.I. Reznikov, A.E. Drobyshevsky, V.I. Kopylov, Russ. Metall. 1 (1981) 971–974.
- [8] R.Z. Valiev, N.A. Krasilnikov, N.K. Tsenev, Mater. Sci. Eng. A 137 (1991) 35–40.
- [9] R.Z. Valiev, R. Chmelik, F. Bordeaux, G. Kapelski, B. Baudelet, Scripta Metall. Mater. 27 (1992) 855–855.
- [10] V.M. Segal, Mater. Sci. Eng. A 197 (1995) 157–164.
- [11] M. Furukawa, Z. Horita, M. Nemoto, R.Z. Valiev, T.G. Langdon, Acta Mater. 44 (11) (1996) 4619–4629.
- [12] S. Ferrasse, V.M. Segal, K.T. Hartwig, R.E. Goforth, Metall. Mater. Trans. A 28A (1997) 1047.
- [13] M.V. Markushev, C.C. Bampton, M.Y. Murashkin, D.A. Hardwick, Mater. Sci. Eng. A 234–236 (1997) 927.
- [14] P. Berbon, N. Tsenev, R.Z. Valiev, M. Furukawa, Z. Horita, M. Nemoto, T.G. Langdon, Metall. Mater. Trans. A 29A (1998) 2237.
- [15] Y. Iwahashi, M. Furukawa, Z. Horita, M. Nemoto, T.G. Langdon, Metall. Mater. Trans. A 29A (1998) 2245.
- [16] T. Mukai, M. Kawazoe, K. Higashi, Mater. Sci. Eng. A 247 (1998) 270–274.
- [17] I.V. Alexandrov, Y.D. Wang, K. Zhang, K. Lu, R.Z. Valiev, in: Z. Liang, L. Zuo, Y. Chu (Eds.), Proceedings of the Conference ICOTOM, vol. 11, 1996, pp. 929–940.
- [18] S.R. Agnew, J.R. Weertman, Mater. Sci. Eng. A 244 (1998) 145–153.
- [19] O.V. Mishin, V.Y. Gertsman, G. Gottstein, in: Z. Liang, L. Zuo, Y. Chu (Eds.), Proceedings of the Conference ICOTOM, Xian, vol. 11, 1996, pp. 1015–1020.
- [20] O.V. Mishin, G. Gottstein, Philos. Mag. A 78 (2) (1998) 373–388.
- [21] S.R. Agnew, U.F. Kocks, K.T. Hartwig, J.R. Weertman, in: J.V. Cartensen, T. Leffers, O.B. Pedersen, B.F. Sorensen, G. Winter (Eds.), Proceedings of the Conference of 19th Risø International Symposium on Material Science, Risø Nat. Lab., Roskilde, Denmark, 1998, pp. 201–206.
- [22] M.A. Gibbs, K.T. Hartwig, L.R. Cornwell, R.E. Goforth, E.A. Payzant, Scripta Metall. 39 (12) (1998) 1699–1704.
- [23] A. Tidu, F. Wagner, T. Grosdidier, W.H. Huang, P.W. Kao, C.P. Chang, in: J.A. Szpunar (Ed.), ICOTOM 12, vol. 1, Montreal, Canada, 1999, pp. 694–699.
- [24] A. Tidu, W.H. Huang, P.W. Kao, T. Grosdidier, C.P. Chang, J. Phys. IV 10 (2000) 10–211.
- [25] W.H. Huang, L. Chang, P.W. Kao, C.P. Chang, Mater. Sci. Eng. A 307 (2001) 113–118.
- [26] L. Dupuy, E.F. Rauch, J.J. Blandin, in: T.C. Lowe, R.Z. Valiev (Eds.), Investigations & Applications of Severe Plastic Deformation, Kluwer, New York, 2000, pp. 189–195.
- [27] I.V. Alexandrov, in: T.C. Lowe, R.Z. Valiev (Eds.), Investigations & Applications of Severe Plastic Deformation, Kluwer, New York, 2000, pp. 103–108.
- [28] J.J. Beyerlein, R.A. Lebensohn, C.N. Tomé, Mater. Sci. Eng. A 345 (2003) 122–138.
- [29] D.P. Delo, T.R. Bieler, S.L. Semiatin, in: R.S. Mishra, S.L. Semiatin, C. Suryanarayana, N.N. Thadhani, T.C. Lowe (Eds.), Ultrafine Grained Materials, MMMS, 2000, pp. 257–265.
- [30] J.W. Sinclair, K.T. Hartwig, R.E. Goforth, E.A. Krenik, E. Voelkl, in: R.S. Mishra, S.L. Semiatin, C. Suryanarayana, N.N. Thadhani, T.C.

- Lowe (Eds.), *Ultrafine Grained Materials*, MMMS, 2000, pp. 393–401.
- [31] U. Chakkingal, A.B. Suriadi, P.F. Thomson, *Mater. Sci. Eng. A* 266 (1999) 241–249.
- [32] J.-H. Han, H.-K. Seok, Y.-H. Chung, M.-C. Shin, J.-C. Lee, *Mater. Sci. Eng. A* 323 (2002) 342–347.
- [33] S.D. Terhune, D.L. Swisher, K. Oh-Ishi, Z. Horita, T.G. Langdon, T.R. McNelley, *Metall. Mater. Trans. A* 33A (2002) 2173–2184.
- [34] M.V. Markushev, M.Y. Murashkin, *Phys. Metals Metall.* 91 (5) (2001) 522–527.
- [35] P.L. Sun, P.W. Kao, C.P. Chang, *Mater. Sci. Eng. A* 283 (2000) 82–85.
- [36] C. Pithan, T. Hashimoto, M. Kawazoe, J. Nagahora, K. Higashi, *Mater. Sci. Eng. A* 280 (2000) 62–68.
- [37] Y.H. Chung, H.D. Kim, H.T. Jeong, O. Engler, M.Y. Huh, *Mater. Sci. Forum* 396–402 (2002) 475–480.
- [38] V.M. Segal, US Patent No. 5,850,755 (1998).
- [39] M. Furukawa, Z. Horita, T.G. Langdon, *Mater. Sci. Eng. A* 332 (2002) 97–109.
- [40] V.M. Segal, US Patent No. 5,513,512 (1996).
- [41] H.R. Wenk, S. Matthies, Beartex, Berkeley Software Package, University of California, Berkeley, 1996.
- [42] U.F. Kocks, in: U.F. Kocks, C.N. Tome, H.R. Wenk (Eds.), *Texture and Anisotropy*, Cambridge University Press, Cambridge, 1988.
- [43] H.R. Wenk, *Preferred Orientations in Deformed Metals and Rocks, An Introduction to Modern Texture Analysis*, Academic Press, New York, 1985.
- [44] H.J. Bunge, *Texture Analysis in Materials Science*, Butterworths, London, 1982.
- [45] S.R. Kalidindi, C.A. Bronkhorst, L. Anand, *J. Mech. Phys. Solids* 40 (1992) 537.
- [46] C.A. Bronkhorst, S.R. Kalidindi, L. Anand, *Phil. Trans. R. Soc. Lond. A* 341 (1992) 443.
- [47] V.M. Segal, *Mater. Sci. Eng. A* 271 (1999) 322–333.
- [48] V.M. Segal, *Mater. Sci. Eng. A* 338 (2002) 331–344.
- [49] V. Andrade, M.A. Meyers, K.S. Vecchio, A.H. Chokshi, *Acta Metall. Mater.* 42 (1994) 3183–3195.
- [50] M.T. Lyttle, J.A. Wert, *J. Mater. Sci.* 29 (1994) 3342–3350.
- [51] F.J. Humphreys, P.B. Prangnell, J.R. Bowen, A. Gholinia, C. Harris, *Phil. Trans. R. Soc. Lond. A* 357 (1999) 1663–1680.
- [52] F.J. Humphreys, M. Hatherly, *Recrystallization and Related Annealing Phenomena*, Pergamon press, Oxford, 1995.
- [53] J. Hirsch, K. Lucke, *Acta Metall. Mat.* 36 (1988) 19–35.
- [54] D.A. Huges, N. Hansen, *Metal. Trans. A* A24 (1993) 2021–2037.
- [55] R.D. Doherty, D.A. Huges, F.J. Humphreys, J.J. Jonas, D. Juul Jensen, M.E. Kassner, W.E. King, T.R. McNelley, H.J. McQueen, A.D. Rollett, *Mater. Sci. Eng. A* 238 (1997) 219–274.
- [56] V.M. Segal, *Mater. Sci. Eng. A* 345 (2003) 36–46.